University of New Hampshire
University of Maine
Sea Grant College Program

DISTRIBUTION OF TIDAL BOTTOM STRESS IN A NEW HAMPSHIRE ESTUARY

by

M. Robinson Swift
Wendell S. Brown

UNH-MP-T/DR-SG-83-2

cation of the UNH/UMe Sea Grant College Program

Distribution of Tidal Bottom Stress in a New Hampshire Estuary

by

M. Robinson Swift
Department of Mechanical Engineering

Wendell S. Brown
Department of Earth Sciences

Report No.: UNH-MP-T/DR-SGF83-2

This work is the result of research sponsored, in part, by the Office of Sea Grant, NOAA, Department of Commerce, under Grant #04-8-M01-79 to the University of New Hampshire. The U.S. Government is authorized to produce and distribute reprints for governmental purposes, any copyright notation that may appear hereon notwithstanding.

The National Science Foundation (Grant #OCE78-26229) and the National Ocean Survey also cooperated in this research.

University of New Hampshire
Durham, N.H. 03824, U.S.A.

February, 1983

Abstract

Estimates of area-averaged, tidal bottom stress are made for four channel segments of the Great Bay Estuary, New Hampshire. Sea level and current measurements are used to estimate pressure gradient and acceleration terms in the equation of motion, while the equation of motion itself is used to infer the remaining stress term. Dynamic terms, bottom stress values, friction coefficients and energy dissipation rates are estimated for each site. To aid in interpreting the results, sea level and current data are subject to a harmonic analysis to determine the tidal constituents at a number of measurement stations located along the estuary's main channel. The variation of current amplitude along the channel axis, which must be evaluated to compute the acceleration terms, is analyzed by considering the distribution of tidal prism and cross-section area.

The results show that at all locations the principal force balance is between the frictional stress and the pressure gradient forcing. RMS values of total bottom stress range from 2.7 to 10.4 N/m^2, while friction coefficients vary from .015 to .054. Energy dissipation was most intense in the seaward portion of the estuary with an order of magnitude decrease at the most inland site.

Introduction

Bottom stress in estuaries and coastal waters can be estimated from current and sea level data using the equation of motion. The data are used to estimate acceleration and pressure gradient terms, and the equation of motion itself is used to infer the remaining bottom stress term. This technique, referred to here as the dynamic inference method, is based on a simplified version of the momentum equation but requires no assumptions regarding a direct relationship between stress and current. Because dynamic terms in the equation of motion are individually estimated, the instantaneous dynamic balances can also be determined.

Bowden and Fairbairn (1952), Bowden et al. (1959) and more recently Wolf (1980) have applied the method to coastal waters to estimate stress, friction coefficients and eddy viscosities. Brown and Trask (1980) have used the method to study a site within a tidal channel. In their formulation the equation of motion is integrated over a channel segment and yields a spatially averaged total stress. Problems of spatial variability, such as those described by Smith and McLean (1977) and Gardner et al. (1979) which plague single point estimates of stress, are avoided. The total stress estimates include both skin friction and the cumulative form drag due to individual roughness elements. The dynamic inference method thus provides a representative estimate of the stress associated with the tidal hydrodynamics.

In this paper the dynamic inference method is applied to four different locations in the main channel of the Great Bay Estuary, New Hampshire. Measurements used include current, sea level, and estimates of volume distribution. Sea level and cross-section averaged current are subjected to harmonic analysis to characterize the estuary's tidal kinematics. The estuary's dynamics are then analyzed to determine how dynamic balances, stress values, friction coefficients and energy dissipation vary with position.

Theoretical Considerations

To obtain spatially averaged bottom stress estimates using the dynamic inference method, the equation of motion must be volume-integrated. In this section the volume-integrated equation of motion is developed for an estuarine channel segment, and the important limitations are outlined. Detailed justification of these equations for application to well-mixed tidal channels has been provided by Brown and Trask (1980). Because the specialized equation of motion contains spatially averaged current terms, a procedure for estimating spatially averaged current from point measurements of current is also discussed.

For the case of a narrow channel having constant density flow with negligible vertical acceleration and effective stresses due to depth variation in current, the vertically averaged equation of motion is

$$\frac{\partial \vec{U}}{\partial t} + \vec{U}\cdot\nabla\vec{U} = -g\nabla\eta - \frac{\vec{\tau}_b}{\rho H} \quad . \tag{1}$$

Here ($\vec{}$) denotes a vector quantity; $\vec{U}$ is the vertically averaged current; η, the surface elevation above mean sea level; $\vec{\tau}_b$, the bottom stress; t, the time; ρ, the density; g, the gravitational acceleration; and H, the depth. Taking the scalar product of this equation with a unit vector parallel to the channel axis results in a longitudinal equation of motion. If $\vec{U}$ and $\vec{\tau}_b$ are directed axially, the longitudinal equation becomes

$$\frac{\partial U}{\partial t} + \frac{\partial}{\partial x}(U^2/2) = -g\frac{\partial \eta}{\partial x} - \frac{\tau_b}{\rho H} \tag{2}$$

where x is an axial coordinate increasing along the channel seaward.

Equation (2) is next integrated over the area of a channel segment. In doing so we assume that longitudinal gradients of current and surface elevation have small variation over the width of the channel and that spatial changes in current, surface elevation and channel width are small with respect to their segment-averaged values. Thus the integrated longitudinal equation of motion becomes

$$\frac{\partial \langle U\rangle}{\partial t} + \frac{\delta(\bar{U}^2/2)}{\delta x} = -g\frac{\delta \bar{\eta}}{\delta x} - \frac{\langle \tau_b\rangle}{\rho H} \tag{3}$$

where $\delta(\ )$ refers to changes over the length of the segment, ($\bar{}$) to cross-section averaged quantities, and $\langle(\ )\rangle$ to segment-averaged quantities. The following rearranged form of Eq. (3) provides an expression for segment-averaged bottom stress, $\langle\tau_b\rangle$,

as a sum of local acceleration (LA), advective acceleration (AA) and pressure gradient (PG) terms:

$$\langle \tau_b \rangle = -\rho H\left[\underbrace{\frac{\partial \langle U \rangle}{\partial t}}_{\text{LA}} + \underbrace{\frac{\delta(\bar{U}^2/2)}{\delta x}}_{\text{AA}} + \underbrace{g\,\frac{\delta \bar{\eta}}{\delta x}}_{\text{PG}}\right] . \qquad (4)$$

The pressure gradient term PG on the right hand side of Equation (4) may be estimated straightforwardly using sea level measurements at each end of the segment. Estimating spatially averaged current values (occurring in the acceleration terms) using point measurements of current, on the other hand, requires additional information on the spatial distribution of current. Consider the problem of estimating $\bar{U}$ using measurements from a single current station consisting of a vertical array of current meters located within the segment. One approach, appropriate for cases of negligible mean flow, is to supplement the current measurement with tidal prism estimates (obtained independently from volume considerations) in the following manner. Cross-section averaged current at the station, $\bar{U}_s$, is assumed proportional to the vertical average of measured current time series, U_v, but with different proportionality constants for the flood and ebb phases to account for tidal asymmetry at the measurement location. Thus

$$\bar{U}_s = C_{Ebb}\, U_v\, H(U_v) + C_{Flood}\, U_v\, H(-U_v) \qquad (5)$$

in which H is the Heaviside step function and the C's are constants. The C's are evaluated by requiring the time integral

of transport over a flood or ebb phase to be equal to the tidal prism so that

$$C_{Ebb} = \frac{Prism}{A\int_{Ebb} U_v dt} \text{ and } C_{Flood} = \frac{Prism}{A\int_{Flood} U_v dt} \tag{6}$$

in which A is the cross-section area.

To estimate current distribution between measurement stations, an average current, U_a, may be computed as a function of longitudinal position x from

$$U_a = \frac{Prism}{A(1/2 \text{ semi-diurnal tidal period})} . \tag{7}$$

The result is a cross-section averaged current which is time-averaged over a flood or ebb phase. Cross-section averaged current $\bar{U}$ at locations other than the current station may then be estimated from $\bar{U}_s$ by assuming that at each cross-section $\bar{U}$ is proportional to U_a. Thus, for example, the segment-averaged current time series is given by

$$\langle U \rangle = \frac{\langle U_a \rangle}{(U_a)_s} \bar{U}_s . \tag{8}$$

Observations

A cooperative field program was carried out by National Ocean Survey (NOS) and the University of New Hampshire (UNH) during the summer and fall of 1975 in the Great Bay Estuary, New Hampshire, which is shown in Fig. 1. The upper part of the estuary, consisting of Great Bay and Little Bay, has extensive

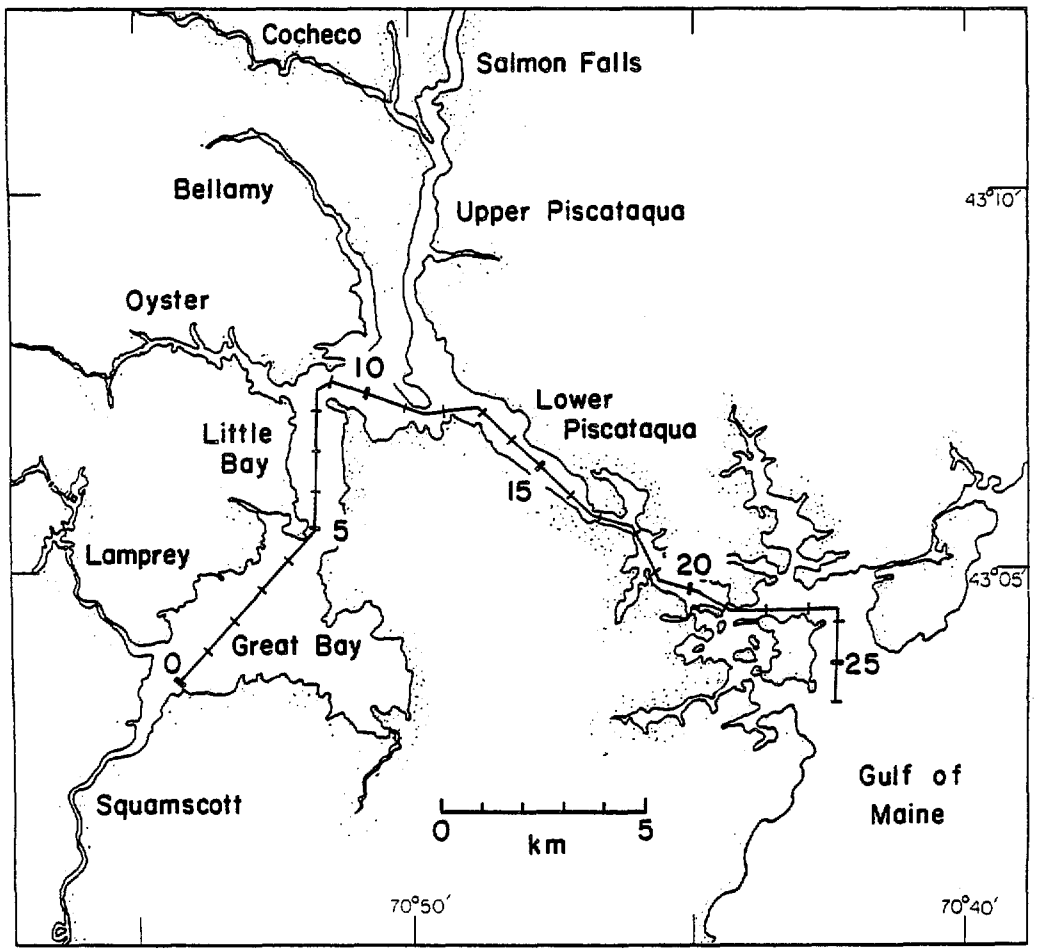

Figure 1. A map of the Great Bay Estuary system situated in southeastern New Hampshire. The axial scale coincides with the estuary's main channel and is divided into kilometers.

mud flat areas and includes several river tributaries. Depths in the main channel are on the order of 10 m and maximum currents are approximately 0.5 m/s. The Upper Piscataqua and its tributaries are less significant to this study because of a much smaller tidal prism. The upper estuary is connected to the Gulf of Maine by the Lower Piscataqua River whose tidal channel has a typical depth of 15 m, and maximum currents in the range from 0.5 to 2 m/s. The estuary is characterized by a low river discharge to tidal prism ratio which during the measurement period was less than 1%. Consequently, density gradients are small, and tidal currents are much larger than the steady-state circulation. Data taken in the NOS/UNH measurement program have been summarized by Swenson et al. (1977) and Silver and Brown (1979).

Measurements of sea level and current used in this study were made at the sites shown in Fig. 2. Most sea level measurements were made by NOS using automatic digital recording tide gauges, which employed a float in a tidal well. The UNH station (T-UNH) used a resistance gauge. Currents were measured by NOS using Savonious rotor current meters deployed at depths of 4.57 m and 9.15 m below MLW where possible. Results from an additional UNH current meter (C-UNH) mounted 0.75 m above the bottom are used in this study. Representative sea level and current data are summarized in Figs. 3 and 4, respectively. The direction of the longitudinal component was determined

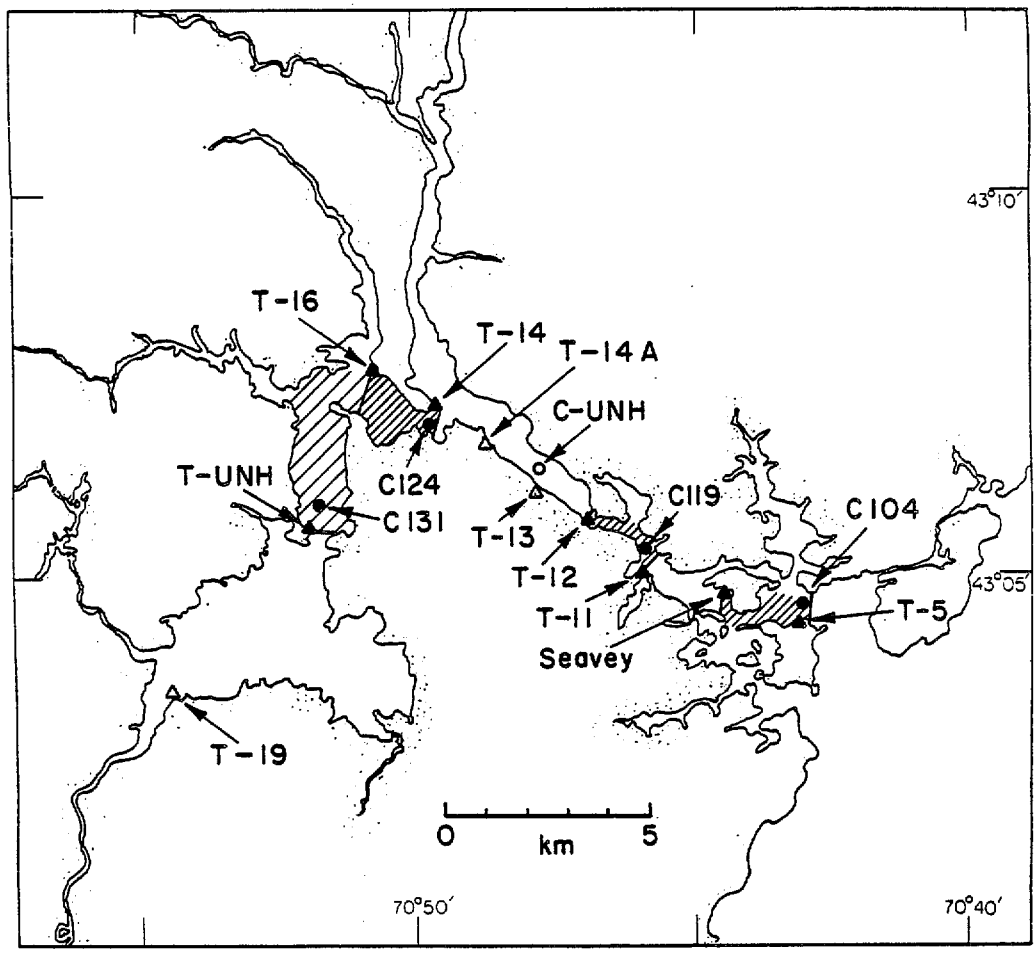

Figure 2. Location map of the tidal elevation stations (▲ and △) and current meter moorings (● and o) in the Great Bay Estuary, NH. Solid symbols indicate current and sea level stations used in the dynamic study of the four hatched areas.

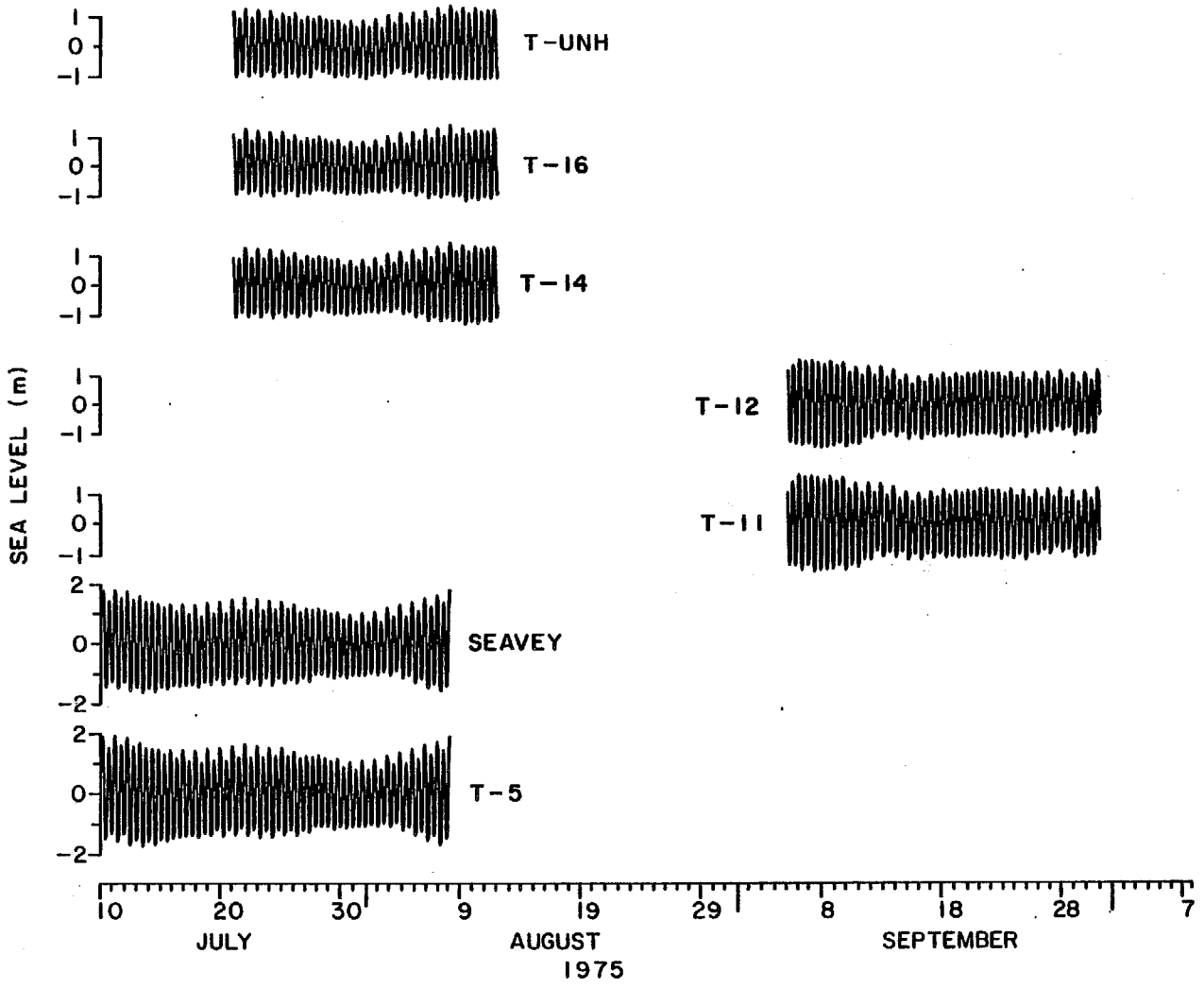

Figure 3. Representative sea level data from the Great Bay Estuary.

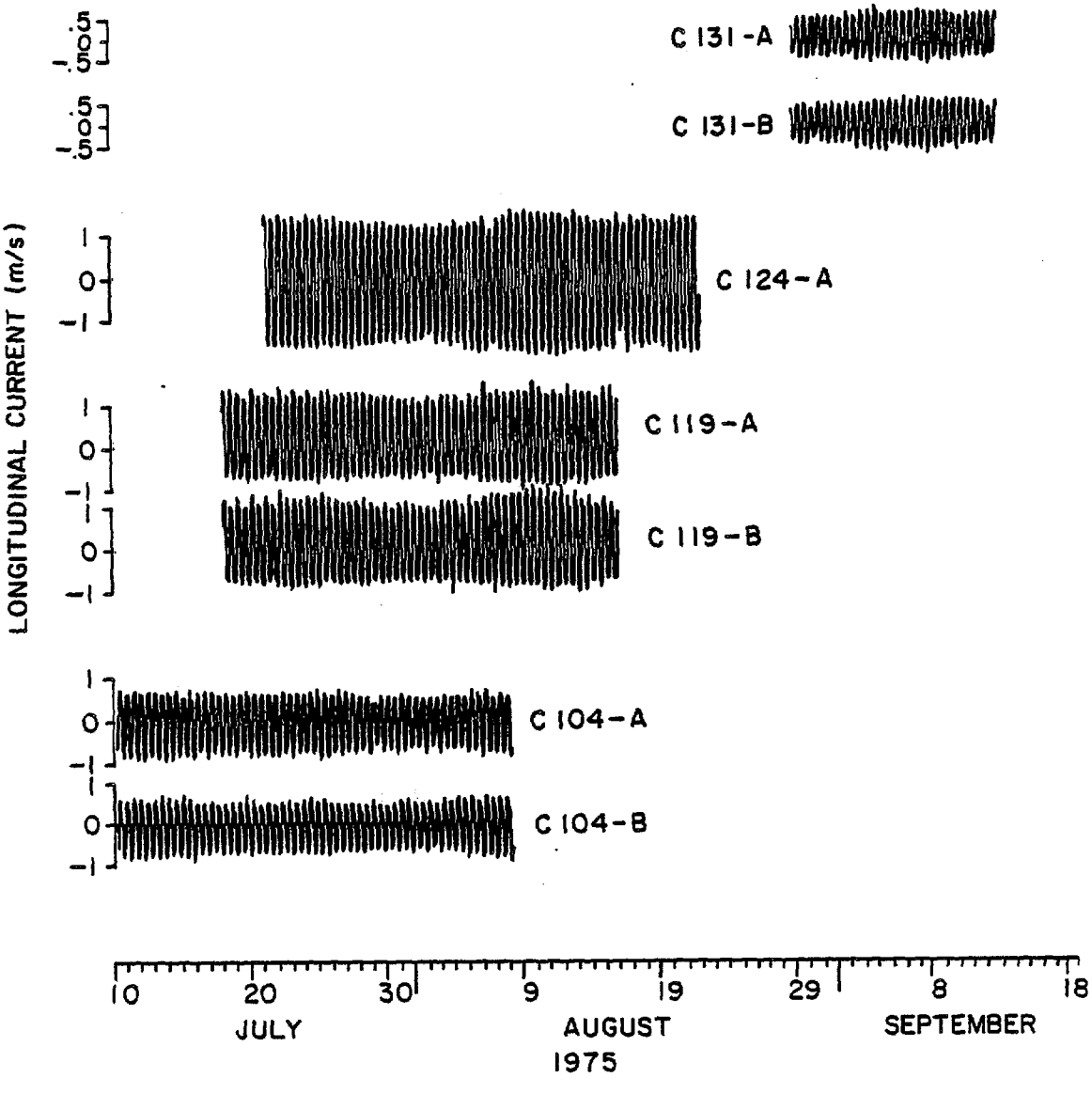

Figure 4. Representative longitudinal current data for the Great Bay Estuary. Suffixes A and B refer to measurements made at depths of 4.75 and 9.15 m below MLW, respectively.

from local topography with the downstream direction considered positive.

Cross-Section Averaged Current

Vertically averaged measurements of current were used to estimate time series of cross-section averaged current using Eqs. (5) and (6) which require tidal prism estimates. Tidal prism was computed from an analysis of low and high water volume distribution and is discussed in Appendix A. This procedure for estimating the cross-section averaged current removes the time-averaged current, but the error is small in the Great Bay estuary since fresh water flow is low.

To determine the current distribution between measurement stations, an average current, U_a, was estimated at half-kilometer intervals using Eq. (7). In Appendix A it is shown how the average tidal currents could be related to maximum tidal currents for both the spring and neap tides. The results are summarized in Fig. 5.

Cross-section averaged currents at arbitrary locations, as required in the AA term of Equation (4), were then computed from the time series of the nearest current station under the assumption that current amplitude is proportional to the local value of U_a. Similarly, the segment-averaged currents, necessary for computing the LA term of Equation (4), were evaluated under the assumption that the segment-averaged amplitude is proportional to $\langle U_a \rangle$ as provided in Equation (8). An analysis

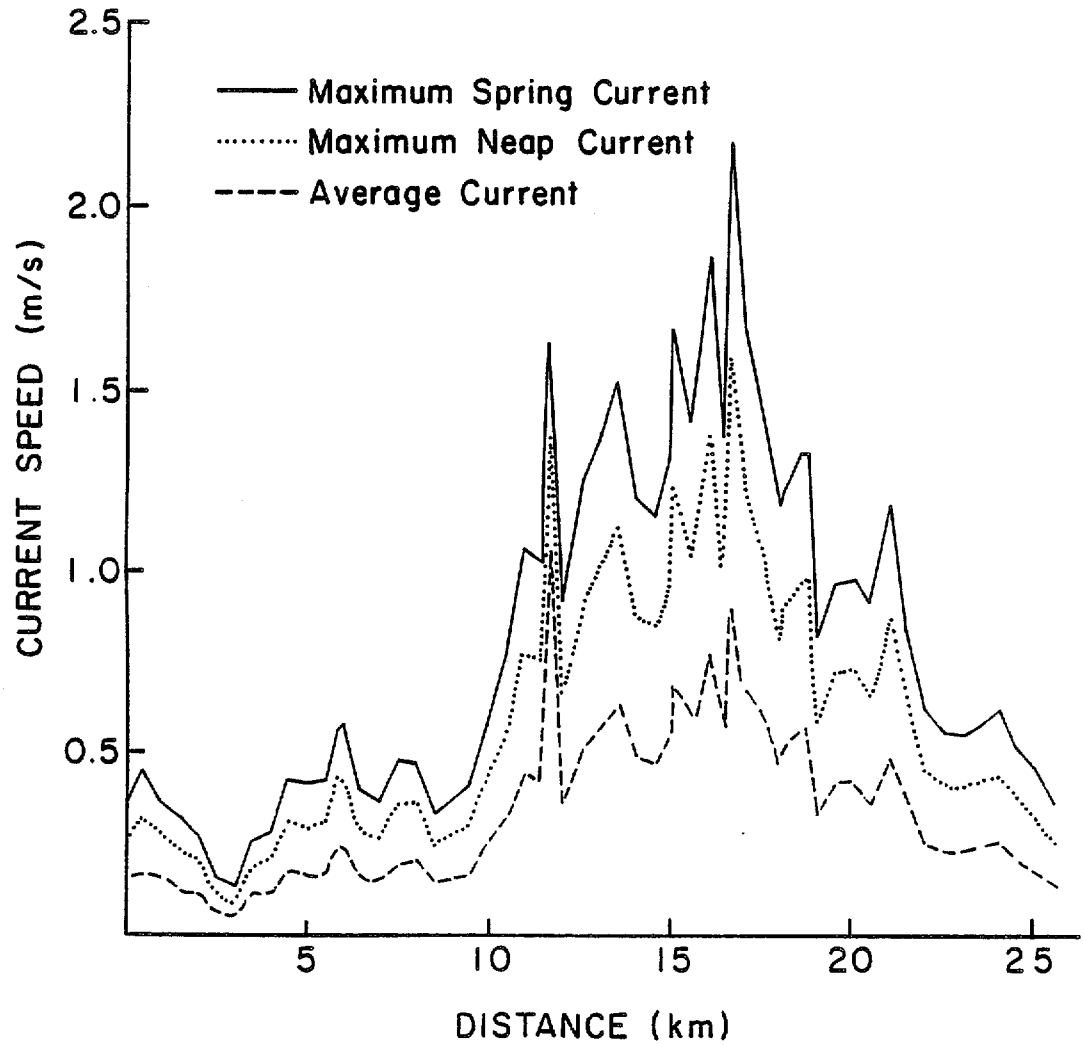

Figure 5. Great Bay Estuary tidal current distribution. Distance corresponds to the axial scale shown in Fig. 1.

of the errors associated with estimating tidal prism and cross-section area distribution in the Great Bay system indicates that the uncertainty in using this procedure is less than $\pm$16%.

Tidal Analysis

A harmonic analysis was performed on sea levels and cross-section averaged currents. The results were obtained using a modified version of the NOS analysis described by Dennis and Long (1971) and are tabulated in Appendix B. Sea level cotidal charts for the principal semi-diurnal, M_2, and diurnal, K_1, constituents are shown in Figs. 6 and 7, respectively. The corresponding cotidal charts for currents appear in Figs. 8 and 9. The amplitudes of the M_2 currents were found to be $1.5 \pm .2$ times the average current U_a at each of the current stations. This result was combined with the average current distribution shown in Fig. 5 to estimate M_2 amplitudes between current stations.

Dynamic Analysis

Estimates of the dynamic terms in Eq. (4) are computed for the four segments shown in Fig. 2. Each segment includes a current station and is identified by the current station designation. Tidal elevation stations bracket the segments at their upstream and downstream ends. Time series for terms on the right-hand side of Eq. (4) are computed for each segment using appropriate sea level and current data (see Figs. 3 and

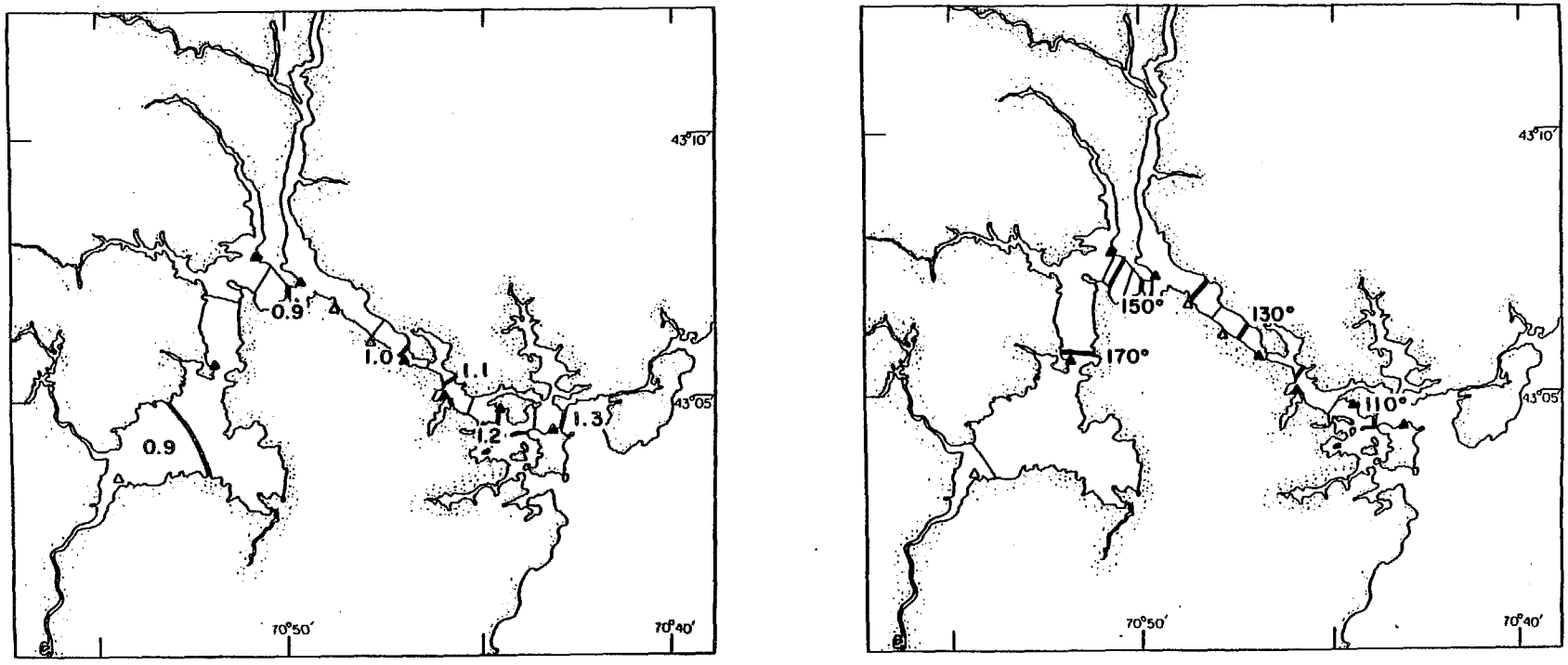

Figure 6. Corange and cophase charts for the M_2 constituent of sea level are shown in (a) and (b), respectively. Amplitudes are in meters, and Greenwich phases are in degrees.

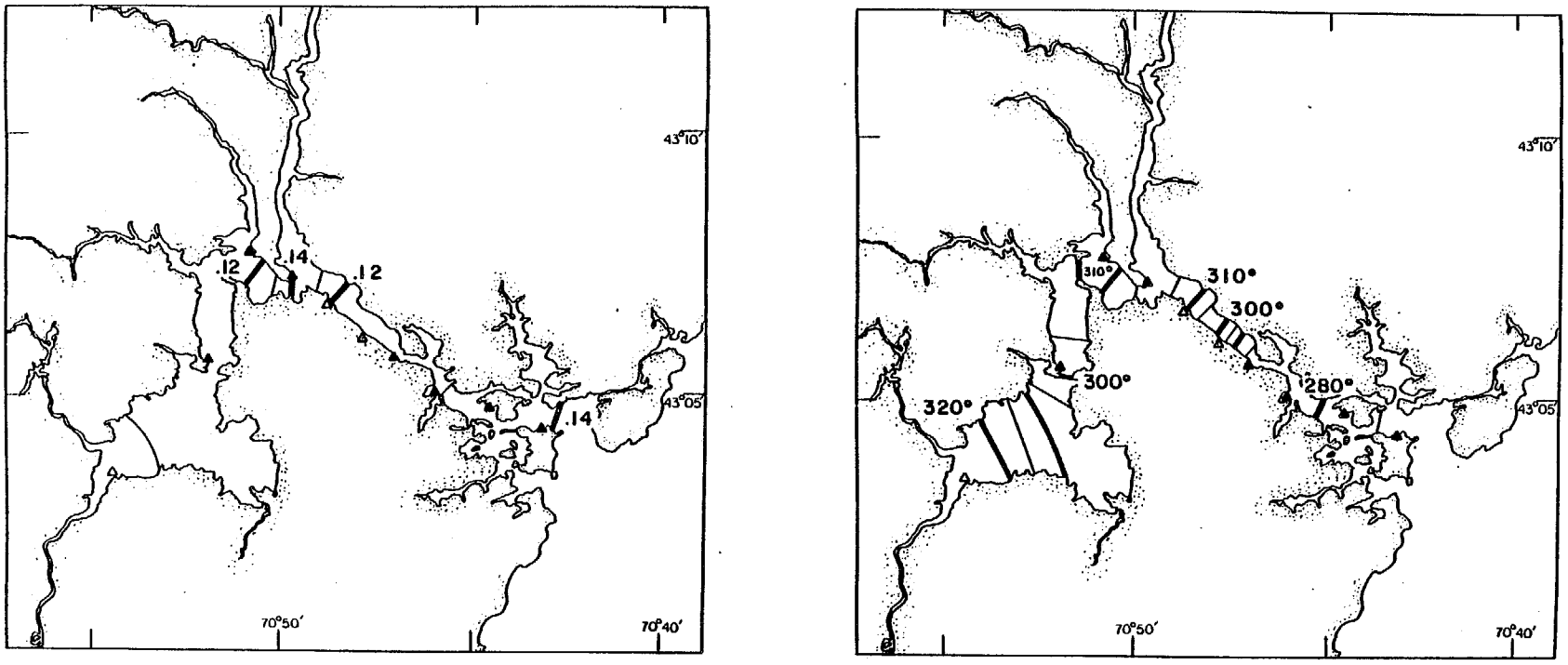

Figure 7. Corange and cophase charts for the K_1 constituent of sea level are shown in (a) and (b), respectively. Amplitudes are in meters, and Greenwich phases are in degrees.

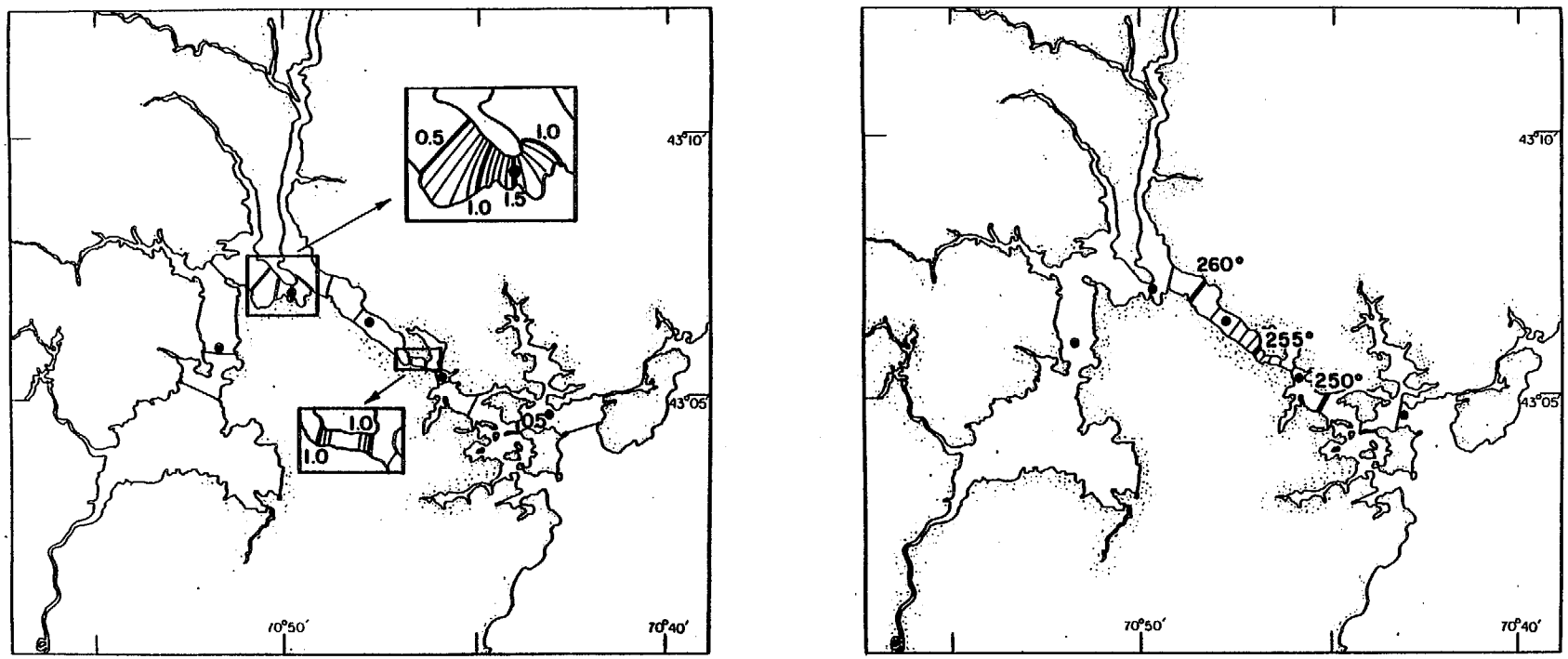

Figure 8. Corange and cophase charts for the M_2 constituent of cross-section averaged, longitudinal current are shown in (a) and (b), respectively. Current amplitudes are in m/s, and Greenwich phases are in degrees. Current amplitudes between current stations, indicated by the dots (•), were determined using the current distribution results shown in Fig. 5.

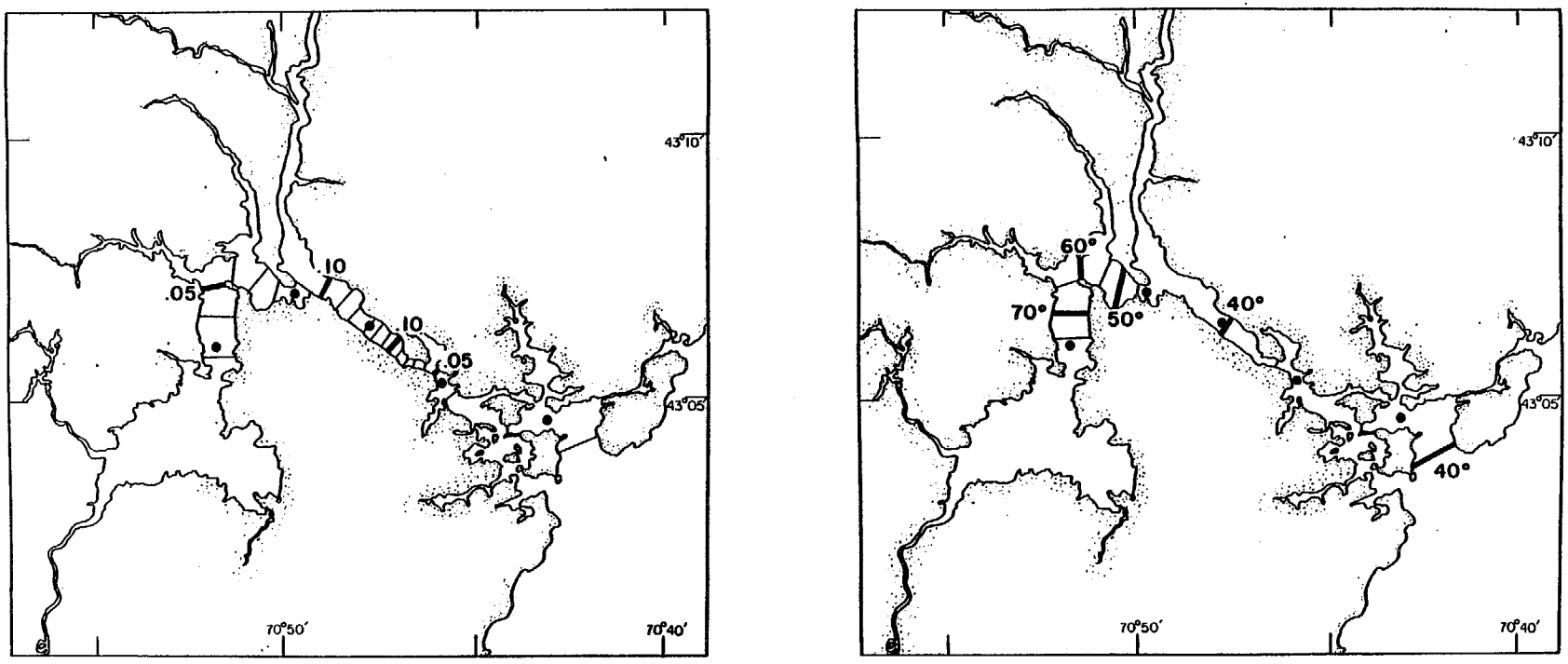

Figure 9. Corange and cophase charts for the K_1 constituent of cross-section averaged, longitudinal current are shown in (a) and (b), respectively. Current amplitudes are in m/s, and Greenwich phases are in degrees.

4). For example, Table 1 outlines how dynamic terms were estimated for segment C119. Current differences and segment averages were estimated using the velocity distribution shown in Fig. 5 and current time series. The pressure gradient term, PG, was estimated from sea level data using relations similar to those in Table 1. For cases where sea level and current data did not coincide, a prediction of PG based on harmonic analysis was computed for the time period of the current observations. Finally, segment-averaged stress is computed according to Eq. (4). Time series of these results for each segment are summarized in Fig. 10.

Friction coefficients C_F were computed as segment-averaged stress divided by the product of density times current velocity squared. Table 2 lists friction coefficients for maximum current calculated using segment-averaged velocities. Also provided is a second friction coefficient C_F' which is based on current at the current measurement sites. Rate of energy dissipation per unit area was estimated as the product of segment-averaged current times segment-averaged stress. Mean dissipation rates and RMS values of stress for each segment are provided in Table 3.

Discussion

These results clearly show that the primary force balance is between the pressure gradient and bottom stress. This is in agreement with the conclusions of Brown and Trask (1980) who

Table 1. Details of dynamic term estimates for segment C119 which extends from sea level station T-12 to T-11 and includes current station C119. (See Fig. 2 for station locations).

Term		Estimate
$-\rho H \frac{\partial \langle U \rangle}{\partial t}$	(LA)	$-\rho H \frac{\langle U_a \rangle}{(U_a)_{C119}} \frac{\partial \bar{U}_{C119}}{\partial t}$
$-\rho H \frac{\delta(\bar{U}^2/2)}{\delta x}$	(AA)	$-\frac{\rho H}{2}\left\{\left[\frac{(U_a)_{T-11}}{(U_a)_{C119}}\right]^2 - \left[\frac{(U_a)_{T-12}}{(U_a)_{C119}}\right]^2\right\} (\bar{U}_{C119})^2 (x_{T-11} - x_{T-12})^{-1}$
$-\rho g H \frac{\delta \eta}{\delta x}$	(PG)	$-\rho g H (\eta_{T-11} - \eta_{T-12}) (x_{T-11} - x_{T-12})^{-1}$

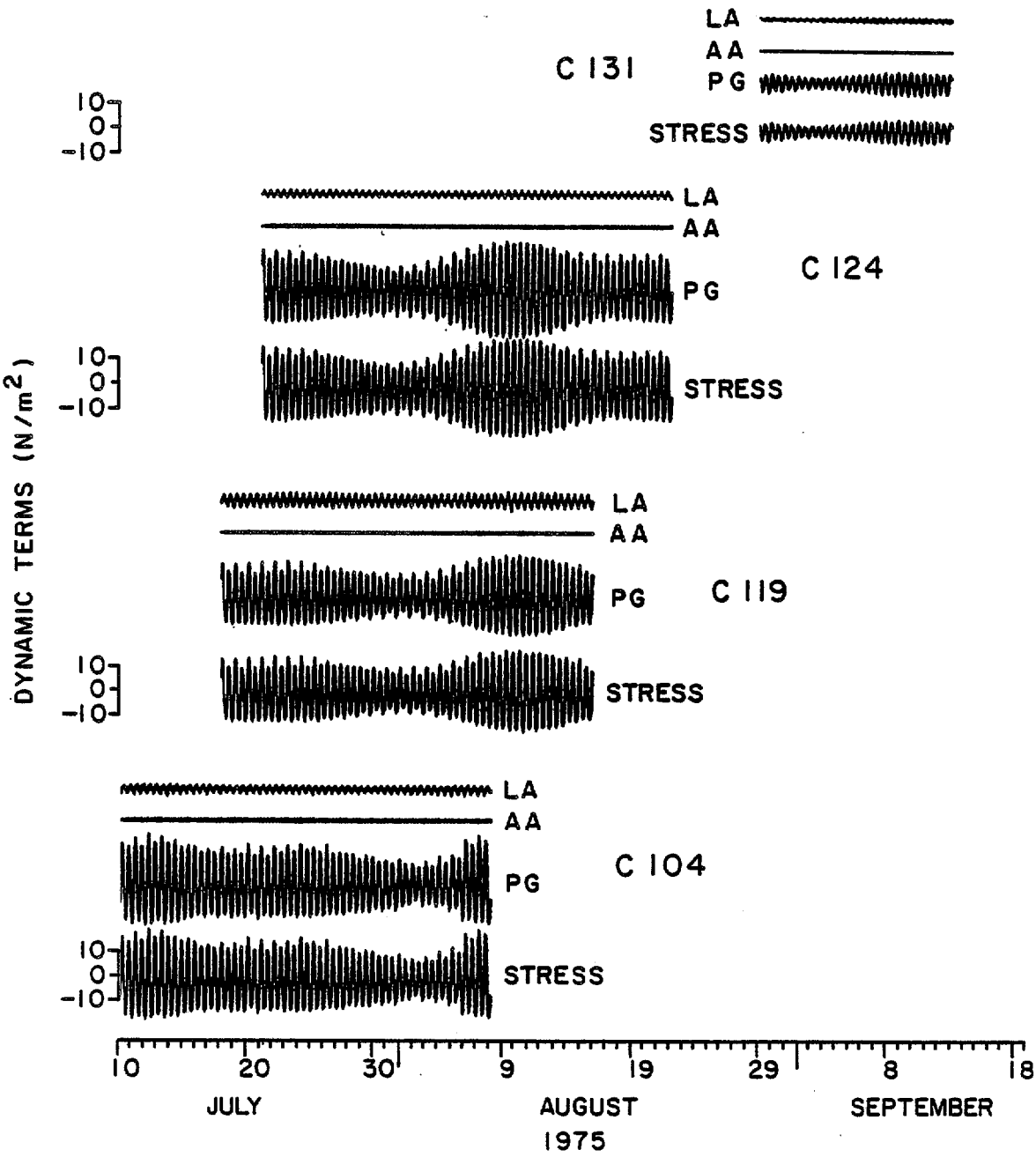

Figure 10. A summary of dynamic analysis time series at four locations in the estuary. The terms are local acceleration (LA), advective acceleration (AA), pressure gradient (PG), and stress ($<\tau_b>$) as defined in Eq. (4). All terms are in units of N/m^2.

Table 2. Summary of friction coefficients. C_F is the segment-averaged friction coefficient defined as $\langle\tau_b\rangle(\rho\langle U\rangle^2)^{-1}$ where $\langle U\rangle$ is the segment-averaged current. C_F' is a friction coefficient defined by $\langle\tau_b\rangle(\rho U_s^2)^{-1}$ where U_s is the cross-section averaged current at the current meter station.

Segment	C_F	C_F'
C131	.038	.023
C124	.035	.007
C119	.015	.025
C104	.054	.063

Table 3. RMS values of segment-averaged stress and mean values of dissipation rate per unit area.

Segment	Stress RMS Value (N/m^2)	Dissipation Mean Value (N/m-s)
C131	2.7 ± .6	.5
C124	10.4 ± 1.1	5.1
C119	8.8 ± 1.8	5.9
C104	9.3 ± 1.9	3.4

applied the same dynamic inference method to a 2 km segment centered at station C-UNH. Thus the pressure gradient/bottom stress balance is maintained throughout the length of the main channel. Experimental results for the Great Bay Estuary are also consistent with a scaling analysis of the equation of motion discussed by LeBlond (1978) which showed that shallow rivers such as the Fraser and St. Lawrence have frictional forces exceeding accelerations over most of the tidal cycle.

Stress values given in Table 3 for segments C124, C119 and C104 are approximately twice as large as the stress estimated by Brown and Trask (1980). Since a major factor in the choice of the C-UNH site was the channel segment's uniformity, lowered stress values are expected. Our stress of 2.67 N/m^2 for segment C131 compares with stress estimates of 2.32 N/m^2 and 3.15 N/m^2 made by Swift et al. (1979) in Little Bay using turbulence measurements and a current profiling technique, respectively. This comparison suggests that segment-averaged stress estimates are representative of local bottom stress values under conditions of slowly varying topography.

All stress values discussed here are total bottom stress values and include both skin friction and form drag due to topographic features and individual roughness elements. Because the skin friction component responsible for initiating sediment movement may be much smaller than the total stress, caution should be taken in using these values directly for

drawing conclusions in connection with sediment transport.

The dynamic analysis presented here has first order accuracy and the results should be interpreted accordingly. The conditions for application of Equation (4) were not satisfied exactly and errors were introduced in estimating terms as summarized in Table 1. For example, the measurements used to estimate terms did not allow computation of steady state contributions. The absolute datum for sea level measurements was not known with sufficient accuracy, so mean pressure gradients were neglected. The method for estimating cross-section averaged velocity also eliminated the time-invariant component. Therefore, second order effects leading to nonlinear residual currents could not be inferred. However, the overall error in these tidal stress estimates due to the neglect of steady state contributions is small and is estimated to be less than 5% at all locations. Similarly, because the LA and AA terms in Equation (4) are both small, errors in estimating cross-section and segment-averaged currents do not contribute significantly to uncertainties in estimating stress. Instead, accuracy is limited primarily by the ability of the tide gauges to resolve small changes in height. Uncertainty estimates for stress from all sources are provided in Table 3.

The dynamic analysis results indicate that, when modeling estuarine processes, it is important to parameterize stress

terms accurately. In this connection Table 2 provides average friction coefficients C_F for each segment. A friction coefficient C_F', based on segment-averaged stress and a single point current measurement, is listed only to show the differences which may arise by using an inappropriate definition. Segment-averaged friction coefficients, with the exception of C119, differ by less than 55%. The lower value of C_F for segment C119 can be explained in part by the distribution of current over the cross-section. Cross-channel transect current measurements reported by Swenson et al. (1977) and dye study results described by Schmidt (1980) indicate that, for much of the Lower Piscataqua between sea level stations T-14A and T-11, currents are concentrated in a narrow core. Velocity gradients near the bottom and sides are lower, resulting in reduced friction coefficients in comparison with other parts of the estuary where more lateral mixing of momentum occurs.

Energy dissipation rates given in Table 3 show that most dissipation takes place in the Lower Piscataqua with an order of magnitude decrease in dissipation upstream from segment C124. In the upper part of the estuary, cumulative prism has decreased so that both current and stress are also much less. The effects of dissipation are seen in the cotidal charts for the M_2 constituent of sea level (see Fig. 6). Amplitude attenuation and phase delay changes are rapid in the Lower Piscataqua, while amplitude and phase above C124 are compara-

tively uniform. The phase of the M_2 constituent of current has similar behavior, as seen in Fig. 8. The direct effects of dissipation on current amplitude, on the other hand, are not readily apparent on the cotidal chart because of the strong dependence of current amplitude on local cross-section area.

Acknowledgements

This work was made possible with the field assistance of Mr. Eric Swenson and Drs. Ronnal Reichard and Barbaros Celikkol. Mr. Richard Trask and Dr. J.D. Irish provided valuable help in the data analysis phase of this effort. Our appreciation is also extended to NOS who acquired much of the sea level and current data used in this study and made it available to us.

This material is based on research supported in part by the Sea Grant Office of the National Oceanic and Atmospheric Administration, U.S. Department of Commerce under Grant No. 04-8-M01-79, while the authors' time spent in manuscript preparation was supported by the National Science Foundation under Grant OCE78-26229.

References

Bowden, K.F. and L.A. Fairbairn, 1952, "A determination of frictional forces in a tidal current," Proc. Roy. Soc., 214, 371-392.

Bowden, K.F., L.A. Fairbairn, and P. Hughes, 1959, "The distribution of shearing stresses in a tidal current," Geophys. J. R. Astr. Soc., 2, 288-305.

Brown, W.S. and E. Arellano, 1979, "The application of a segmented tidal mixing model to the Great Bay Estuary, N.H.," UNH Sea Grant Technical Report UNH-SG-162, 47 pp.

Brown, W.S. and R.P. Trask, 1980, "A study of tidal energy dissipation and bottom stress in an estuary," J. Phys. Ocean., 10, 1742-1754.

Dennis, R.E. and E.E. Long, 1971, "A user's guide to a computer program for harmonic analysis of data at tidal frequencies," NOAA Technical Report NOS41.

Gardner, G.B., A.R.M. Nowell and J.D. Smith, 1979, "Turbulent processes in estuaries," Wetland and Estuarine Processes and Water Quality Modeling Workshop, U.S. Army Corp of Engineers, New Orleans.

LeBlond, P.H., 1978, "On tidal propagation in shallow rivers," J. Geophys. Res., 83, 4717-4721.

Munk, W.H. and D.E. Cartwright, 1966, "Tidal spectroscopy and prediction," Phil. Trans., A, 259, 533-581.

Schmidt, E., 1980, "Dispersion studies in the Piscataqua River," UNH Sea Grant Technical Report UNH-SG-167, 42 pp.

Silver, A.L. and W.S. Brown, 1979, "Great Bay estuarine field program 1975 data report part 2: temperature, salinity and density," UNH Sea Grant Technical Report UNH-SG-163, 59 pp.

Smith, J.D. and S.R. McLean, 1977, "Spatially averaged flow over a wavy surface," J. Geophys. Res., 82, 1735-1746.

Swenson, E., W.S. Brown and R.P. Trask, 1977, "Great Bay estuarine field program 1975 data report Part 1: currents and sea levels," UNH Sea Grant Technical Report UNH-SG-157, 109 pp.

Swift, M.R., R. Reichard and B. Celikkol, 1979, "Stress and tidal current in a well-mixed estuary," ASCE J. Hydraul., 105, 785-799.

Wolf, J., 1980, "Estimation of shearing stresses in a tidal current with application to the Irish Sea," In: Marine Turbulence, J.C.J. Nihoul(ed), Elsevier, Amsterdam, 319-344.

Appendix A

Volume, Area and Current Distribution

Table A1 lists volume, area and current distribution for the Great Bay Estuary. Cumulative low water volume (LWV), cumulative high water volume (HWV), cumulative prism and cross-section area were estimated for average conditions in the spring/neap cycle using NOS sea level data, NOS charts and UNH bathymetry data reported by Swenson et al. (1977). The volume and area distributions presented here are primarily based on estimates made for the main channel by Brown and Arellano (1979). Their results were modified for this study to include volume distribution for the whole system. Added to Brown and Arellano's (1979) estimates were volume contributions due to river tributaries (listed separately in Table A2), and a prism contribution of 4.96×10^6 m^3 which enters the channel south of the main estuary axis at 21.2 km on the estuarine scale shown in Fig. 1 of the main text. Fig. A1 shows low and high water volume distribution, plotted from Table A1, while Fig. A2 depicts cumulative prism and cross-section area.

Table A1. Cumulative volume, area and velocity distribution for the Great Bay Estuary, NH. Distance corresponds to the channel axis scale shown on the location map, Fig. 1. LWV and HWV are the cumulative low water volume and high water volume, respectively, for average conditions. Prism is HWV minus LWV. Area is estuary cross-section area. Average current is prism divided by the product of area times one half of the semi-diurnal tidal period. At distances of 5.8, 11.6, 18.0 and 22.8 km, maximum neap and spring currents were obtained directly from current measurements. Values at other points were obtained using average current and the average ratios of (maximum neap current) (average current)$^{-1}$ = 1.77, and (maximum spring current) (average current)$^{-1}$ = 2.41.

Distance (km)	LWVx10^{-6} (m^3)	HWVx10^{-6} (m^3)	Prismx10^{-6} (m^3)	Area (m^2)	Average Current (m/s)	Maximum Neap Current (m/s)	Maximum Spring Current (m/s)
0.0	2.20	7.33	5.13	1440	.159	.281	.383
0.5	2.52	8.45	5.93	1420	.187	.331	.451
1.0	2.93	9.65	6.72	1920	.157	.278	.378
1.5	3.37	11.13	7.76	2580	.135	.239	.325
2.0	3.90	13.19	9.29	3580	.116	.205	.280
2.5	4.48	16.20	11.72	7780	.067	.119	.161
3.0	6.45	22.02	15.57	13740	.051	.090	.123
3.5	11.32	30.89	19.57	7980	.110	.195	.265
4.0	13.96	36.23	22.27	8560	.116	.205	.280
4.5	16.61	40.15	23.54	6100	.173	.306	.417
5.0	18.43	44.43	26.00	6880	.169	.299	.407
5.5	21.05	47.69	26.64	6980	.171	.303	.412
5.8	22.81	50.12	27.31	5120	.239	.438	.563
6.0	23.98	51.74	27.76	5080	.244	.432	.588
6.5	26.19	54.61	28.42	7640	.166	.294	.400
7.0	29.49	58.96	29.47	8580	.154	.273	.371
7.5	33.33	63.70	30.37	6820	.199	.352	.480
8.0	36.24	67.62	31.38	6980	.201	.356	.484
8.6	41.13	77.38	36.25	11760	.138	.244	.333
9.4	46.33	83.94	37.61	9960	.169	.299	.407
9.9	51.35	93.57	42.22	7780	.243	.430	.586
10.4	54.73	97.97	43.24	6020	.321	.568	.774
10 9	57.38	101.35	43.97	4460	.441	.781	1.063
11.4	58.44	102.95	44.51	4680	.425	.752	1.024
11.6	59.29	103.98	44.69	1860	1.075	1.375	1.625
11.9	60.55	105.52	44.97	5380	.374	.662	.901
12.6	74.42	128.46	54.04	4680	.517	.915	1.246
13.1	76.42	131.15	54.73	4300	.569	1.007	1.371
13.6	78.16	133.20	55.04	3840	.629	1.113	1.516
14.1	79.89	135.83	55.94	5020	.498	.881	1.200
14.6	82.16	138.57	56.41	5300	.476	.843	1.147
14.8	83.08	139.73	56.65	4660	.544	.963	1.311
15.1	84.48	141.48	57.00	3700	.689	1.220	1.660
15.6	87.10	144.57	57.47	4380	.587	1.039	1.415
16.1	89.11	146.95	57.84	3340	.774	1.370	1.865
16.5	90.37	148.37	58.00	4530	.573	1.014	1.382
16.6	90.68	148.72	58.04	2880	.901	1.595	2.171
17.1	92.08	150.21	58.13	3780	.689	1.220	1.660

Table A1. Continued

Distance (km)	LWVx10^{-6} (m^3)	HWVx10^{-6} (m^3)	Prismx10^{-6} (m^3)	Area (m^2)	Average Current (m/s)	Maximum Neap Current (m/s)	Maximum Spring Current (m/s)
17.6	93.96	152.11	58.15	4420	.588	1.041	1.417
18.0	95.62	153.98	58.36	5420	.482	.813	1.188
18.1	96.04	154.45	58.41	5140	.508	.899	1.224
18.6	98.38	157.25	58.87	4780	.551	.975	1.328
18.8	99.20	158.34	59.14	4770	.552	.977	1.330
19.1	100.43	159.97	59.54	7960	.335	.593	.807
19.6	102.95	164.55	61.60	6760	.408	.722	.983
20.1	105.90	168.36	62.46	7340	.378	.669	.911
20.6	109.26	172.34	63.08	8060	.350	.620	.844
21.1	112.17	176.29	64.12	6240	.459	.812	1.106
21.6	115.53	185.36	69.83	9040	.346	.612	.834
22.1	119.68	190.24	70.56	12140	.260	.460	.627
22.6	125.26	196.80	71.54	13500	.237	.419	.571
22.8	127.79	199.68	71.89	10300	.313	.563	.750
23.1	131.58	203.99	72.41	14260	.227	.402	.547
23.6	138.00	211.84	73.84	13740	.240	.425	.578
24.1	144.29	219.30	75.01	13380	.251	.444	.605
24.6	150.27	226.69	76.42	15920	.215	.381	.518
25.1	156.91	235.98	79.07	19440	.182	.322	.439

Table A2. Tributary contributions to the Great Bay Estuary cumulative volume distribution.

Location	LWVx10^{-6} (m^3)	HWVx10^{-6} (m^3)	Prism x 10^{-6} (m^3)
Squamscott	1.88	6.47	4.58
Lamprey	.32	.86	.54
Oyster	2.00	4.82	2.82
Bellamy	1.24	3.70	2.46
Upper Piscataqua	11.47	19.64	8.17

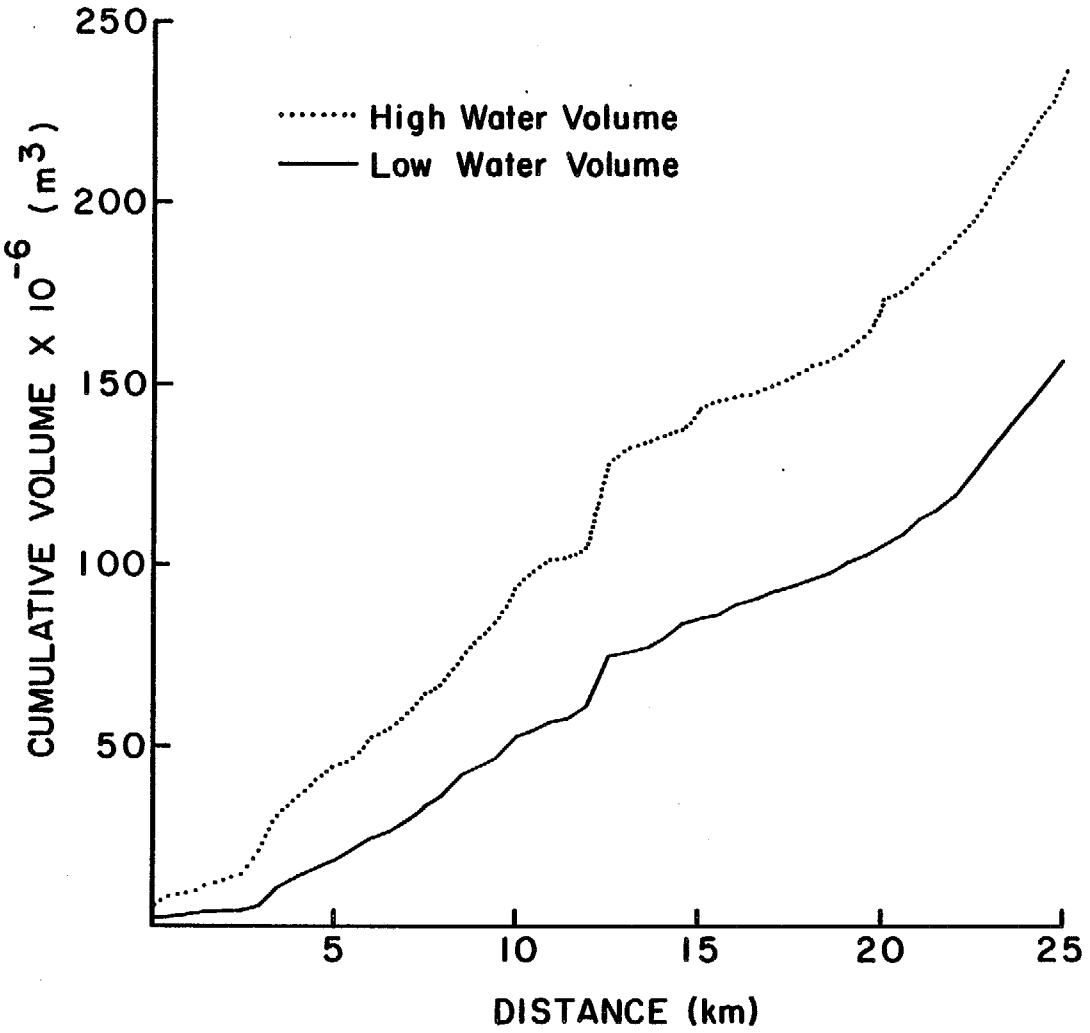

Figure A1. Great Bay Estuary cumulative volume distribution. Distance corresponds to the axial scale shown in Fig. 1 of the main text.

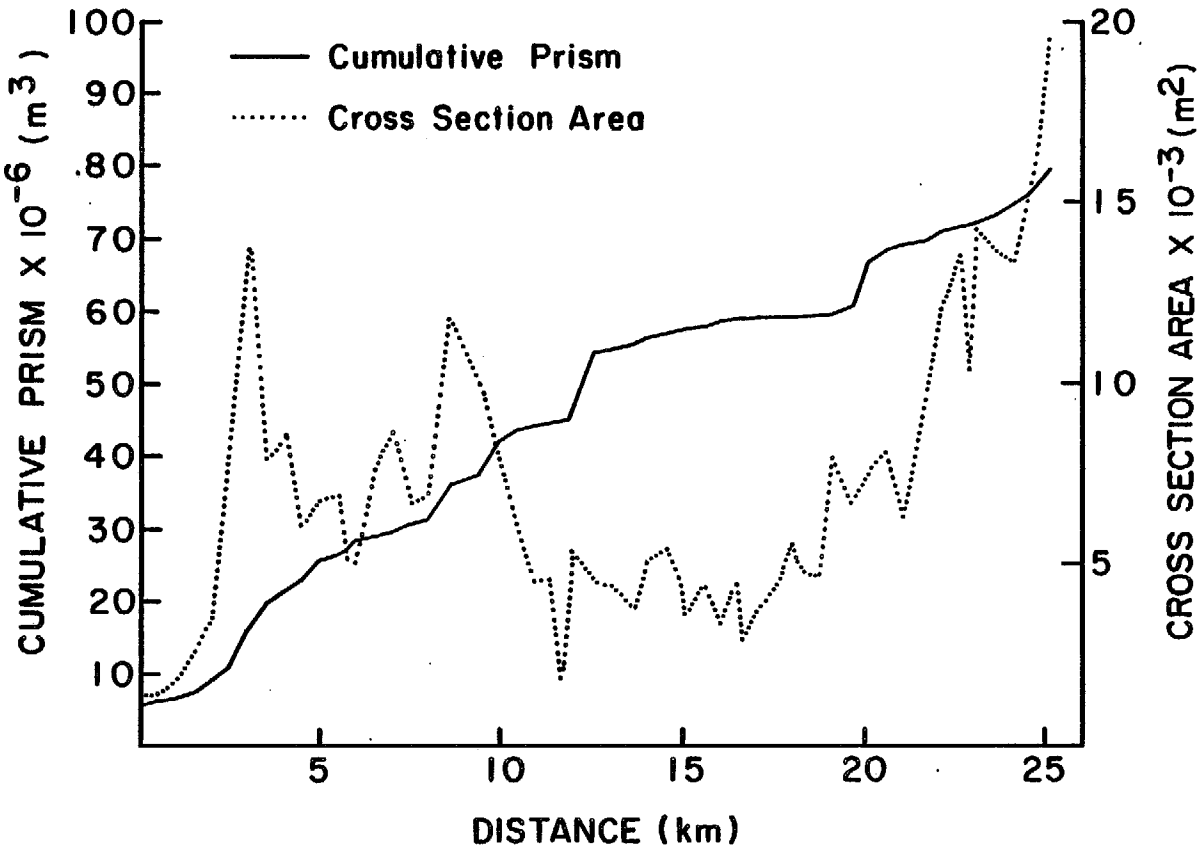

Figure A2. Great Bay Estuary cumulative prism and cross-section area distribution. Distance corresponds to the axial scale shown in Fig. 1 of the main text.

The distribution of average current listed in Table A1 was obtained by dividing cumulative prism by cross-section area times one half the semi-diurnal tidal period. The average current, therefore, represents a current spatially averaged over the channel cross-section and time-averaged over half a semi-diurnal tidal cycle during average conditions in the spring/neap cycle. The average current at each tidal station was then compared to maximum current during both neap and spring tide conditions. Ratios of maximum current to average current are given in Table A3. Ratios at different stations, with the exception of C124, are seen to be consistent (within 10%). The inconsistency of C124 is explained in part by its very small cross-section area (see Fig. A2 at 11.6 km). C124 was, therefore, omitted in computing "average" maximum current to average current ratios. The "average" maximum current to average current ratios were then used to infer maximum current distributions for both neap and spring tidal conditions. Maximum and average current distributions given in Table A1 are plotted in Fig. 5 of the main text.

Table A3. Ratios of maximum current during neap and spring conditions to average current. Station C124 was neglected in calculating average ratios.

Station	$\frac{\text{Maximum Neap Current}}{\text{average current}}$	$\frac{\text{Maximum Spring Current}}{\text{average current}}$
C131	1.83	2.36
C124	1.28	1.51
C119	1.69	2.46
C104	1.80	2.40
average ratios	1.77	2.41

Appendix B

Tidal Analysis

Harmonic constituents were obtained for sea level and cross-section averaged current using a modified version of the harmonic analysis method described by Dennis and Long (1971). The 95% confidence limits were estimated for the dominant M_2 constituent using a method adapted from procedures outlined by Munk and Cartwright (1966). They relate error estimates to a noise parameter defined as the ratio of background noise energy density in the frequency domain at the semi-diurnal tidal frequency to the corresponding value for tidal energy. The noise parameter is then used to find amplitude and phase uncertainties from figures found in Munk and Cartwright (1966).

The results of the tidal analysis are listed in Tables B1 and B2 for constituents found to be significant. Constituents considered significant had sea level amplitude greater than 1 cm or current amplitude greater than 1 cm/sec.

Table B1. Summary of principal sea level harmonic constituents for locations in the Great Bay Estuary, N.H. The parameters κ and G are local and Greenwich epoch, respectively. The amplitude and phase uncertainties (see text) are shown for the M_2 constituent only. The variances for the observed and residual signal are included.

Constituents	T-UNH 43° 05.4'N 70° 51.9'W Amplitude (m)	κ (deg)	G (deg)	T-16 43° 07.8'N 70° 50.8'W Amplitude (m)	κ (deg)	G (deg)	T-14 43° 07.3'N 70° 49.7'W Amplitude (m)	κ (deg)	G (deg)
M_2	.87±.04	29±2	171±2	.83±.04	24±2	166±2	.94±.03	3±2	145±2
S_2	.13	80	221	.07	51	193	.12	38	179
N_2	.19	342	124	.18	344	126	.21	335	116
K_1	.11	160	301	.11	172	313	.14	162	303
O_1	.10	145	287	.09	147	288	.10	134	275
M_4	.03	158	300	.01	252	34	.03	153	294
M_6	.02	50	191	.03	79	220	.02	48	189
Recorded variance (m^2)	4.59×10^{-1}			4.82×10^{-1}			5.23×10^{-1}		
Residual variance (m^2)	2.08×10^{-2}			2.20×10^{-2}			9.60×10^{-3}		

Constituents	T-12 43° 05.8'N 70° 47.0'W Amplitude (m)	κ (deg)	G (deg)	T-11 43° 05.1'N 70° 45.8'W Amplitude (m)	κ (deg)	G (deg)	Seavey 43° 04.8'N 70° 44.5'W Amplitude (m)	κ (deg)	G (deg)
M_2	1.00±.03	346±2	128±2	1.12±.03	336±1	117±1	1.20±.02	333±1	114±1
S_2	.15	29	170	.15	10	152	.17	8	149
N_2	.23	318	99	.25	308	90	.28	306	87
K_1	.13	140	282	.13	140	282	.13	138	279
O_1	.10	131	273	.11	123	264	.11	121	262
M_4	.03	101	243	.03	69	210	.02	99	241
M_6	.01	100	242	.01	61	202	.01	117	259
Recorded variance (m^2)	6.05×10^{-1}			7.06×10^{-1}			8.16×10^{-1}		
Residual variance (m^2)	1.97×10^{-2}			7.44×10^{-3}			7.43×10^{-3}		

Table B1. Continued.

T-5
43° 04.4'N
70° 43.1'W

Constituents	Amplitude (m)	κ (deg)	G (deg)
M_2	1.29±.02	325±1	106±1
S_2	.19	359	140
N_2	.30	297	78
K_1	.14	132	274
O_1	.12	115	256
M_4	.02	52	193
M_6	.01	84	226
Recorded variance (m^2)	9.36×10^{-1}		
Residual variance (m^2)	7.39×10^{-3}		

Table B2. Summary of significant current harmonic constituents. The parameters κ and G are local and Greenwich epoch, respectively. The amplitude and phase uncertainties (see text) are shown for the M_2 constituent only. The variances for the observed and residual signal are included.

	C131 43° 06.0'N 70° 51.7'W			C124 43° 07.0'N 70° 49.7'W			C119 43° 05.5'N 70° 45.8'W		
Constituents	Amplitude (m)	κ (deg)	G (deg)	Amplitude (m)	κ (deg)	G (deg)	Amplitude (m)	κ (deg)	G (deg)
M_2	.31±.01	120±2	261±2	1.48±.08	120±3	262±3	.70±.03	109±3	248±3
S_2	.03	186	328	.19	168	309	.10	160	286
N_2	.06	124	266	.26	99	241	.12	96	225
K_1	.03	294	76	.09	262	44	.04	265	44
O_1	.02	212	354	.08	254	35	.04	254	32
M_4	.03	267	49	.04	18	159	.02	89	248
M_6	.05	182	324	.14	189	330	.07	180	318
Recorded variance $(m/s)^2$	6.82×10^{-2}			1.26×10^{0}			1.28×10^{-1}		
Residual variance $(m/s)^2$	3.17×10^{-3}			5.11×10^{-2}			4.575×10^{-3}		

	C104 43° 04.6'N 70° 43.0'W		
Constituents	Amplitude (m/s)	κ (deg)	G (deg)
M_2	.47±.02	107±3	248±3
S_2	.05	144	286
N_2	.10	84	225
K_1	.03	263	44
O_1	.02	251	32
M_4	.04	107	248
M_6	.03	176	318
Recorded variance $(m/s)^2$	1.28×10^{-1}		
Residual variance $(m/s)^2$	4.58×10^{-3}		